Epithelial heme oxygenase-1 enhances colonic tumorigenesis by inhibiting ferroptosis

Rosemary C. Callahan[1,3,4], Geetha Bhagavatula[5,6,7], Jillian Curry[1,3,4], Alyse W. Staley[6,8], Rachel E. M. Schaefer[1,3,4], Faiz Minhajuddin[1,3], Liheng Zhou[1,3], Rane Neuhart[1,3], Shaikh M. Atif[2,3], David J. Orlicky[9], Ian M. Cartwright[1,3,4], Mark Gerich[1,3], Arianne L. Theiss[1,3,4], Caroline H. T. Hall[5,6,7], Sean P. Colgan[1,3,4], and Joseph C. Onyiah[1,3,4,#]

[1]Division of Gastroenterology and Hepatology; [2]Division of Allergy and Clinical Immunology; [3]Department of Medicine, University of Colorado School of Medicine, Aurora, CO;

[4]Rocky Mountain Regional Veterans Affairs Medical Center, Aurora, CO;

[5]Division of Gastroenterology, Hepatology and Nutrition; [6]Department of Pediatrics, University of Colorado School of Medicine; [7]Children's Hospital Colorado, Aurora, CO;

[8]University of Colorado Cancer Center Biostatistics Core, Aurora, CO;

[9]Department of Pathology, University of Colorado School of Medicine, Aurora, CO.

[#] Corresponding author: Joseph C. Onyiah, M.D.

University of Colorado School of Medicine
Rocky Mountain Regional VA Medical Center
12700 East 19th Ave. MS B-146, Aurora, CO 80045
Phone: (303) 724-8130; Email: joseph.onyiah@cuanschutz.edu

*The authors have declared that no conflict of interest exists.

Abstract

Colorectal cancer has been linked to chronic colitis and red meat consumption, which can increase colonic iron and heme. Heme oxygenase-1 (*Hmox1*) metabolizes heme and releases ferrous iron, but its role in colonic tumorigenesis is not well-described. Recent studies suggest that ferroptosis, the iron-dependent form of cell death, protects against colonic tumorigenesis. Ferroptosis culminates in excessive lipid peroxidation that is constrained by the antioxidative glutathione pathway. We observed increased mucosal markers of ferroptosis and glutathione metabolism in the setting of murine and human colitis, as well as murine colonic neoplasia. We obtained similar results in murine and human colonic epithelial organoids exposed to heme and the ferroptosis activator erastin, especially induction of *Hmox1*. RNA sequencing of colonic organoids from mice with deletion of intestinal epithelial *Hmox1* (*Hmox1*$^{\Delta IEC}$) revealed increased ferroptosis and activated glutathione metabolism after heme exposure. In a colitis-associated cancer model we observed significantly fewer and smaller tumors in *Hmox1*$^{\Delta IEC}$ mice compared to littermate controls. Transcriptional profiling of *Hmox1*$^{\Delta IEC}$ tumors and tumor organoids revealed increased ferroptosis and oxidative stress markers in tumor epithelial cells. In total, our findings reveal ferroptosis as an important colitis-associated cancer signature pathway, and *Hmox1* as a key regulator in the tumor microenvironment.

Introduction

The chronic relapsing-remitting mucosal inflammation of inflammatory bowel disease results in recurrent epithelial damage and repair, significantly increasing the risk of dysplasia and cancer when compared to the general population (1-3). The risk is greatest for those who have colitis, such as Crohn's colitis or ulcerative colitis (UC), and is dependent on the extent of tissue involved, disease activity and duration of disease (4-6). Common symptoms of UC include abdominal pain, diarrhea, and hematochezia. Clinical severity scores in UC, such as the Mayo Clinic Score typically include an assessment of the degree of hematochezia as part of a disease activity index (DAI) (7, 8). Bleeding in the context of inflammation results in damaged extravascular erythrocytes, which release substantial amounts of hemoglobin and heme. Heme consists of a protoporphyrin ring with a central ferrous iron (Fe^{2+}) atom. Studies have shown that hemoglobin and heme-iron can facilitate the formation of reactive oxygen species resulting in DNA damage, neoplastic transformation, or cell death (9-12). Epidemiological to preclinical studies have linked increased dietary heme, typically from red meat consumption, with epithelial hyperplasia and increased risk of colon cancer (13, 14). Tissues protect against heme toxicity by efficiently binding and transporting away excess free heme or by intracellular metabolization (15). The heme oxygenase (HO) group of enzymes, including rapidly inducible HO-1, metabolize heme into equimolar amounts of carbon monoxide (CO), biliverdin and ferrous iron, which is subsequently rendered inert by binding to ferritin (16). If an excess of redox-active labile ferrous iron occurs, it can lead to activation of the iron-dependent cell death pathway termed ferroptosis, a phenomenon that has recently been associated with heme exposure in intestinal epithelial cells (10, 17). Unchecked ferroptosis ultimately results in lipid peroxidation and cell death. The glutathione pathway, anchored by GPx4, acts as a counterbalance to ferroptotic activity (18). It is increasingly recognized as both pathogenic and protective depending on the disease context, including in the setting of neoplasia (19, 20). In this study we report that inducible HO-1 in colonic epithelial cells is an endogenous regulator of ferroptosis, and that it facilitates survival of neoplastic epithelial cells in a ferroptotic tumor microenvironment (TME).

Results

Inflammation triggers ferroptosis in the colon

In human chronic colitis and murine experimental models of colitis, severe mucosal injury and inflammation is associated with bleeding, a common symptom that increases exposure of colonic epithelium to heme. In the murine dextran sodium sulfate-induced (DSS) colitis model, a DAI score typically comprises changes in body weight, visible fecal blood, and fecal softness (21). The DAI score typically increases during DSS injury (Fig. 1A). We observed a temporal relationship between duration of DSS injury, fecal bleeding score and measured fecal heme content, which decreased once DSS was withdrawn on day 5 in our model (Fig. 1B-C). Heme is an inducer of the HO-1/CO pathway, and in murine colitis this has been identified as protective (22-24). We examined colonic *Hmox1* as a marker of the protective mucosal response in our colitis model and observed a significant increase during the course of DSS injury, correlating with our observation of increased bleeding and fecal heme content (Fig, 1D). We also examined mRNA expression of several reported markers of ferroptosis including *Ptgs2, Slc7a11, Chac1* and *Gpx4* (19). We observed a similar temporal increase in gene expression of these markers over the course of DSS injury (Fig. 1E), suggesting increased ferroptosis activity. Consistent with prior reports, colonic tissue from colitic mice demonstrated patchy but increased detection of the lipid peroxidation marker 4-hydroxynonenal (4-HNE) (Fig. 1F), especially in regenerating epithelium exposed to the intestinal lumen (25, 26). We examined a publicly available Gene Expression Omnibus data set (GSE38713) that has previously reported transcriptional patterns in healthy colon tissue, actively or inactively inflamed tissue, as well as uninvolved adjacent colon from UC patients (27). We observed a similar elevation of ferroptosis-linked gene expression particularly in actively inflamed tissue from UC patients (Fig. 1G). To confirm these findings, we prospectively collected colon biopsy tissue from UC patients and similarly measured increased expression of key ferroptosis markers compared to healthy controls (Fig. 1G). Our findings suggest that colitis promotes a ferroptotic environment resulting in a protective response in both human and murine colon, possibly in response to colitis-associated hemorrhage and heme.

Heme induces a ferroptotic response in colonic epithelial organoids

Given the vital role of colonic epithelial cells in the response to intestinal injury, we examined their specific response to inducers of ferroptosis using colonic epithelial stem cell-derived organoids (colonoids) we developed from naïve WT C57BL/6 mice (Fig. 2A). We exposed them to hemin (hemin = heme-Fe^{3+}) and the well-established ferroptosis inducer, erastin, which prevents glutathione synthesis by blocking System X_C^- the cystine/glutamate antiporter encoded by *Slc7a11* and *Slc3a2* (20). We confirmed induction of lipid peroxidation by detecting increased 4-HNE in colonoids treated with hemin (Fig. 2B). We then examined expression of ferroptosis response genes (Fig. 2C). We observed increased expression of genes including *Slc7a11, Fth1, Ttl1, Hmox1, Gstp1* and *Gclm* in both erastin and hemin exposed cells. *Gpx4* and *Slc3a2* were induced only in erastin exposed cells, while *Hmox1* was induced more robustly with heme exposure. We examined HO-1 expression in $CD45^-EpCAM^+$ IECs during DSS colitis using flow cytometry. Like *Hmox1* expression in the colonoids and in the whole tissue, we detected increased IEC HO-1 in response to DSS injury (Fig. 2D). Prior studies have demonstrated *HMOX1* and HO-1 expression by IHC in the colon of patients with ulcerative colitis, including lamina propria mononuclear cells and the epithelium (28-30). We additionally measured increased HO-1 levels in human colonic mucosal biopsies of patients with UC compared to controls using ELISA (Fig. 2E). We examined *Hmox1* expression in colonoids developed from human colonic epithelial stem cells (Fig. 2F). We observed marked upregulation of *Hmox1* expression and *Slc3a2* in response to erastin and heme, while other markers of ferroptosis were less robustly increased (Fig. 2G). These findings reveal that heme is an inducer of ferroptosis in murine and human colonic epithelial cells and *Hmox1* a consistent biomarker of this response.

Loss of colonic epithelial *Hmox1* dysregulates glutathione metabolism and promotes ferroptosis

Given the cytoprotective function of *Hmox1* and its consistent expression in pro-ferroptotic contexts, we examined the impact of its deletion on colonic epithelial responses. We bred previously described C57BL/6 *Hmox1*$^{fl/fl}$ mice (31) with *Vil1*-cre expressing mice (32) to produce IEC specific deletion of

Hmox1 expression (*Hmox1*$^{\Delta IEC}$ or knockout/KO mice) (Fig. S1A). Colonic epithelial stem cells were used to develop *Hmox1* deficient colonoids (Fig. 3A). Like prior reports in human colonic epithelial cell lines (10), we found that loss of *Hmox1* led to increased cell death in murine colonoids upon exposure to moderate amounts of heme (Fig. 3B). Using colonoids derived from *Hmox1*$^{fl/fl}$ and *Hmox1*$^{\Delta IEC}$ mice, we examined transcriptional responses underlying the cytoprotective role for HO-1 in the setting of heme exposure, by means of mRNA sequencing. Significantly different and shared gene expression patterns were seen between KO and control colonoids, and in response to heme (Fig. 3C-D). Around 900 genes were upregulated in the *Hmox1*$^{fl/fl}$ colonoids exposed to heme relative to *Hmox1*$^{\Delta IEC}$ colonoids, while almost 800 were increased in the *Hmox1*$^{\Delta IEC}$ colonoids (Fig. 3E). Kyoto Encyclopedia of Genes and Genomes (33) pathway analysis revealed many pathways that were significantly upregulated in the KO colonoids exposed to heme compared to the controls (Fig. 3F). The most highly significant pathway was glutathione metabolism, and the closely related ferroptosis pathway was also very significantly regulated (Fig. 3F). When we examined the expression of specific genes in these pathways, we found a pattern highly consistent with increased oxidative stress in the *Hmox1* deficient cells, characterized by significant upregulation of glutathione pathway and ferroptosis response genes (Fig. 3G). We confirmed these findings by qPCR analysis of a similar subset of these genes in a separate experiment (Fig. S1B). Depletion of glutathione has previously been shown to trigger cell cycle arrest in retinal pigment epithelial cells, while inhibition of HO-1 has been associated with G1 arrest in a human intestinal epithelial cell line and in HO-1 deficient macrophages (10, 34, 35). We examined cell cycle progression in our colonoids in the presence and absence of heme (Fig. S1C) and observed an increased fraction of KO cells in the G0/G1 phase relative to controls with increased levels of heme (Fig. S1C). These findings suggest that HO-1 plays a key protective role in heme-exposed colonic epithelial cells, and its loss increases the risk of oxidative stress, ferroptosis and cell cycle arrest.

The colonic tumor microenvironment promotes ferroptosis

Increased resistance to oxidative stress is a well-established characteristic of developing tumors. Upregulation of a network of oxidative stress response pathways is seen in both human and murine neoplasms, facilitating cancer stem cell proliferation and protecting against damage or cell death from reactive oxygen species (36). Despite this, colorectal cancer epithelial cells have been shown to have an avidity for iron, which supports tumor metabolism and growth, and yet can also promote ferroptotic cell death (37, 38). In line with this balance, a recent study observed that inhibiting ferroptosis in the context of the murine azoxymethane + DSS (AOM-DSS) colitis-associated cancer model allowed for significantly increased number and size of tumors (26). We examined markers of iron metabolism and ferroptosis/oxidative stress in the AOM-DSS model comparing matched tumors to adjacent uninvolved colon tissue from WT C57BL/6 mice (Fig. 4A). In support of prior findings, genes important for iron import, such as *Tfrc* and *Slc11a2,* had elevated expression in the tumors compared to the uninvolved adjacent colon, while the sole iron exporter *Slc40a1*/ferroportin expression was downregulated, as has been seen by IHC in a mouse model of sporadic CRC (37). This would explain increased cellular iron retention. Consistent with this, we also observed simultaneously increased expression of several ferroptosis linked genes in the tumors, such as *Ptgs2, Slc7a11, Slc3a2, Gclm, Hmox1* and *Gpx2,* consistent with increased ferroptotic activity or response. Also, 4-HNE staining of AOM-DSS tumors confirms active lipid peroxidation in this microenvironment (Fig. 4B).

Deletion of colonic epithelial *Hmox1* constrains colitis-associated tumorigenesis

We further examined the influence of IEC *Hmox1* using the AOM-DSS colitis-associated cancer model, where a carcinogen is used in combination with three rounds of colitis and recovery (Fig. 5A). This is a chronic/recurrent model of colonic injury, and the repeated epithelial injury and recovery promotes dysplasia and the development of multiple tumors over several weeks (39). We did not observe a clinical difference between our control *Hmox1*$^{fl/fl}$ mice and our *Hmox1*$^{\Delta IEC}$ mice during acute or chronic colitis, including in bleeding or fecal heme content (Figs. 5B; S2). After we retrieved the colons a the

end of the experiment, tumors were examined visually (Fig. 5C). We observed a significant decrease in the numbers of visible colonic tumors in the *Hmox1*$^{\Delta IEC}$ mice (Fig. 5D). Injury in this model can be patchy but often the severity is worse in the mid-distal colon (21). The location of tumors in both mouse strains favored the distal half of the colon, consistent with this observation (Figs. 5E; S3A). There was a slightly higher rate of proximal tumors in the *Hmox1*$^{fl/fl}$ mice (25.8% vs 14.9%) (Fig. S3B). The tumor burden, as measured by total surface area of tumors involved, was decreased in the *Hmox1*$^{\Delta IEC}$ mice and the tumors were on average significantly smaller than in the control mice (Fig. 5F-H), while a similar relationship was seen for estimated tumor volume (Fig. S3C-D). Changes in body weight during the experiment were similar between the two groups of mice, and the overall level of histologic colonic injury was similar at the end of the experiment (Fig. 5I). Overall, this suggests that the difference in numbers of tumors, and tumor size, is not driven by decreased inflammation, which is often the case in this model. Just as the visual appearance of the tumors did not appear consistently different on gross examination, no obvious differences in tumor appearance were noted microscopically (Figs. 5J; S3E). There were similarities in the proportions of dysplastic lesions, adenomas, and adenocarcinomas between the mice (Fig. S3F). Collectively, these results suggest that loss of *Hmox1* in colonic epithelial cells decreases growth of tumors but not neoplastic progression of established tumors.

<u>Tumor epithelial cells from *Hmox1*$^{\Delta IEC}$ tumors show increased susceptibility to ferroptosis/oxidative stress</u>

To gain better insight into the behavior of specific cell populations in the tumor microenvironment, we performed comparative single cell RNA-sequencing (scRNA-seq) on pooled tumors isolated from *Hmox1*$^{fl/fl}$ and *Hmox1*$^{\Delta IEC}$ mice. We recovered and pooled all tumors > 2mm in diameter, and after enzymatic digestion to recover single cells, we sorted the entire population of live cells. We performed scRNA-seq using the 10X Genomics platform and data was analyzed in R using Seurat version 4.3.0 (Fig. 6A). Approximately 24,000 cells passed quality control and after library normalization and dimensionality reduction, cells were co-embedded in UMAP space. Unsupervised clustering initially

identified 18 different clusters, which we further clarified using known classic marker genes (e.g. T cells: *CD3e*; B cells: *CD79a*; tumor epithelial cells: *Epcam*; neutrophils: *Cxcr2*; monocyte/macrophages: *Fcgr1*; mast cells: *Fcer1a*), and prior reports of scRNA-seq in AOM-DSS and murine intestine (Figs. 6B-C; S4) (40-42). Clusters from the two mouse strains were overall similar, consisting of populations of tumor epithelial cells and a broad range of leukocytes including T cells, NK cells, B cells, mast cells, neutrophils, monocytes, macrophages, dendritic cells, plasma cells and a small population of basophils (Fig. 6B). We observed that there were noticeably less tumor epithelial cells, and more leukocytes as a percentage of the total cells from *Hmox1*$^{\Delta IEC}$ mouse tumors compared to control mice (Fig. 6D). We also noted similar findings when examining the tumor leukocyte fraction in a larger cohort of mice by flow cytometry, suggesting decreased relative epithelial survival or increased leukocyte recruitment (Fig. 6E). This CD45^{+} leukocyte fraction had a strong inverse correlation with tumor burden (Fig. 6E). We examined gene expression in the *Epcam*$^{+}$ tumor epithelial cell subcluster, based on Gene Ontology processes: *response to oxidative stress* and *glutathione metabolism* (43). Several ferroptosis and oxidative stress response genes showed higher expression in *Epcam*$^{+}$ cells from *Hmox1*$^{\Delta IEC}$ mice (Fig 6F), including *Ptgs2*, *Slc7a11, Txnrd1*, and *Cdkn1a,* which was recently linked to cell cycle arrest and sensitivity to ferroptosis (44). We further examined the susceptibility of tumor epithelial cells from *Hmox1*$^{fl/fl}$ and *Hmox1*$^{\Delta IEC}$ mice by developing a 3D tumor organoid model using murine tumor epithelial stem cells (tumoroids). After exposure to heme in vitro we observed significant upregulation of ferroptosis/oxidative stress response genes in tumoroids from *Hmox1*$^{\Delta IEC}$ mice consistent with pattern seen in the scRNA-seq (Fig. 6G).

Discussion

Gastrointestinal cancers continue to be a major contributor to the increasing burden of cancer on a global scale (45, 46). Ferroptosis is a recently described non-apoptotic form of cell death that is increasingly recognized as playing a role in progression of gastrointestinal cancers, including CRC (47). While CRC growth is fueled by sequestration of iron, excess labile iron can also promote oxidative

stress and ferroptotic cell death (37, 38). Hence the need for CRC epithelial cells to upregulate oxidative stress pathways to manage this risk (36). Our expanding understanding of cell death and survival pathways is improving our knowledge of mechanisms employed by cancer cells to thrive in otherwise suboptimal environments (36). As we learn more about iron metabolism and ferroptosis in CRC, there remain gaps in our understanding of additional endogenous factors that influence the onset and response to ferroptosis.

While the focus of ferroptosis has often been on increased labile iron, there is clear evidence that heme-iron is very redox-active in either the heme-Fe^{2+} or heme-Fe^{3+} oxidation state (48, 49). Heme-bound iron can likely participate in Fenton-like and other reactions, leading to lipid peroxidation, which underscores the importance of protective HO-1 in the setting of heme exposure (48). For example, studies have shown that exposure of colonic epithelial cells to hemoglobin and heme result in increased reactive oxygen species, DNA damage and cell death that is exacerbated with blockade or loss of HO-1 function (9, 10). There is also evidence to suggest that dietary heme contributes to colonic tumorigenesis (12, 14). Dietary heme significantly interferes with homeostasis of the colonic epithelium by causing colonocyte damage, increasing the mucosal inflammatory response and markedly inhibiting epithelial apoptosis, resulting in an abnormal epithelial hyperproliferation and hyperplasia response (50, 51).

Far less is known mechanistically about heme and epithelial HO-1 in the tumor microenvironment. Our studies using murine and human colonoids, colonic tissue and tumors, identify HO-1 as a prominent signature of inflammatory and oxidative stress that tracks with induction of ferroptosis. Both inflammation and neoplasia can compromise tissue and vascular integrity, with the resulting hemorrhage and released heme triggering induction of HO-1. However, other factors such as inflammatory cytokines, bacterial antigens and hypoxia/HIF signaling may contribute to HO-1 induction, including in the TME (52). Our studies suggest that in *Hmox1*$^{\Delta IEC}$ cells, the diminished ability to induce HO-1 in response to these factors, metabolize heme, and sequester the redox-active iron with ferritin, contributes to increased ferroptosis, thereby reducing survival and growth in the colitis-associated

cancer context. However, there has been inconsistency with regards to the role of HO-1 as a suppressor or promoter of ferroptosis in other studies, but this may be contextual with regards to cell type, iron source and regulation of pertinent transcription factors such as Bach1 (53-55). In addition, while there is evidence that HO-1 can inhibit the inflammatory response in epithelial cells (56, 57), there is conflicting evidence that ferroptosis can contribute to both anti-tumor immunity and immune suppression, underlying the need to better understand how these pathways interact (58-60).

In summary, our results support the role of IEC *Hmox1* as an endogenous regulator of ferroptosis in colonic tumorigenesis, facilitating survival of cancer epithelial cells in a ferroptotic microenvironment. Continued examination of survival pathways in digestive cancers can unlock mechanistic targets that we can leverage in a therapeutic context.

Methods

DSS colitis vs Azoxymethane-DSS colitis. C57BL/6J WT mice were used where indicated and C57BL/6 *Hmox1*$^{fl/fl}$ mice were kindly provided by Dr. H. B. Suliman (31). *Hmox1*$^{\Delta IEC}$ mice were made by crossing *Hmox1*$^{fl/fl}$ mice with B6.Cg-Tg(Vil1-cre)1000Gum/J mice expressing Cre recombinase in villus and crypt epithelial cells of the small and large intestines (JAX #021504) (32). All mice were maintained and managed in accordance with Institutional Animal Care and Use Guidelines. Littermate controls were used for all colitis experiments. We used age-matched male and female mice between age 7 and 14 weeks. A single dose of AOM at 10 mg/kg of body weight was administered intraperitoneally on day 0 were indicated. Mice were given 2.5% colitis grade dextran sodium sulfate (DSS, MP Biomedical) in drinking water, changed every 2 days, for 5 days. Mice were sacrificed at day 7 where indicated otherwise mice received 14-days of tap water followed by a second 5-day course of 2.5% DSS in drinking water, followed by a 14-day rest period, then a third 5-day course of 2.5% DSS in drinking water followed by a final 28-day water only period. Mice were sacrificed on day 80. Disease activity components were measured blindly (weight change, stool consistency, and hematochezia scores; scale 0-3) and an index was computed by summing the scores (max score of 9). At experiment end, colons

were excised, cleaned, the lumen was then exposed, and photos were taken with ruler or calipers for measurements of the tumors. Final tumor measurements (e.g. area) were calculated using ImageJ (61). Colons were embedded and processed for histology. H&E stained tissue was scored by a histo-pathologist blinded to the treatments and groupings of animals using described methods (21).

IEC/leukocyte isolation and flow cytometry. Isolation of tumor cells and intestinal epithelial cells was performed as previously described (62). Modifications include retention of the dissociated epithelial fraction where necessary for fluorescence activated cell sorting (FACS) and measurement of *Hmox1* expression. We performed flow cytometry as previously described (62). Dead cells were stained and excluded using BioLegend 7AAD viability staining solution or Zombie Aqua™ dye prior to flow cytometry or FACS. Anti-4-HNE (R&D Systems) was used with an AF647 secondary antibody (Invitrogen) to detect lipid peroxidation via flow cytometry, which was validated using H_2O_2 as a positive control. Other anti-mouse antibodies were purchased from BioLegend or Thermo Fisher Scientific: CD45 (30-F11); EpCAM (G8.8). Flow cytometry was performed on a FACSCanto™ II (Becton Dickinson), or a BD FACSAria™ Fusion and resulting data was analyzed with De Novo's FCS Express 7 software.

Cell culture. Epithelial cells were harvested from 8 to 12-week-old *Hmox1*$^{fl/fl}$ and *Hmox1*$^{\Delta IEC}$ mice and processed as previously described to make colonoids and tumor organoids (63). Media was supplemented L-WRN and with ROCK inhibitor Y-27632. Hemin was purchased from Sigma-Aldrich. Erastin was purchased from MedChemExpress. Viability of tumor organoids was assayed using RealTime-Glo™ MT Cell Viability Assay by Promega with heme treated organoids compared to their baseline activity.

Reverse transcription-quantitative PCR (qPCR) and mRNA sequencing. RNA was isolated from snap frozen tissue samples or cells using Trizol (Invitrogen) or Qiagen RNeasy Mini kit respectively, with the addition of the gDNA-eliminator columns as per manufacturer's protocol. First-strand complementary DNA synthesis was performed with using iScript reverse transcription super-mix from Bio-Rad. Real-

time qPCR was performed using SYBR green on Applied Biosystems QuantStudio 5 Real-Time PCR System. β-Actin (*Actb*) was used as the reference gene and results are reported as ΔCt, which is the Ct of the target gene subtracted from the Ct of the reference gene (higher ΔCt values = higher expression relative to the reference gene). Primer sets were purchased from Sigma-Aldrich's KiCqStart™ line. Preparation of mRNA library, sequencing and bioinformatic analysis was conducted by Novogene Corporation Inc.

Heme quantification assay. Total heme was measured using an established protocol with minor adaptations (64).

Immunohistochemistry. Paraffin-embedded sections of tissue were analyzed for 4-hydroxynonenal as previously described (65). 4-HNE antibody was purchased from R&D Systems. Representative photomicrographs were obtained using an EVOS m5000 microscope.

Human colonic biopsy tissue. Patient colon biopsy samples were collected during colonoscopy and made available as part of a biobank repository at the University of Colorado Anschutz Medical Campus Crohn's and Colitis Center with Colorado Multiple Institutional Review Board approval. ELISA for HO-1 was performed using a human HO-1 DuoSet IC kit from R&D Systems, and total protein was assessed using a Pierce™ BCA Protein Assay Kit.

NCBI Gene Expression Omnibus. In data set GSE38713, colonic gene expression in patients with ulcerative colitis and non-inflammatory controls was assayed using Affymetrix GeneChip high-density oligonucleotide HGU133 Plus 2.0 microarrays (27). Initial analysis was performed using GEO2R with $\log_2$ transformation and *P*-values were adjusted using Benjamini and Hochberg FDR method (66). Only probe sets that represent a single gene (labeled as *_at) were used.

Single cell RNA sequencing.

Processing: Processing and statistical analyses were performed in R version 4.2. (67) and Seurat version 4.3.0 (68). Seurat defaults were used unless otherwise noted. The data were restricted to

features with at least 3 detected cells and low-quality cells with more than 15% mitochondrial genes or less than 300 genes were filtered out. The DoubletFinder package version 2.0.3 (69) was then used to remove multiplets. This yielded 23,698 high quality cells across two *Hmox1*$^{fl/fl}$ and two *Hmox1*$^{\Delta IEC}$ mice. Library size normalization was performed with NormalizeData and the top 2000 highly variable genes (HVGs) were identified with the FindVariableFeatures variance stabilizing transformation (VST) method. Features that were repeatedly variable across datasets were then used as anchors to create an integrated dataset across samples with the FindIntegrationAnchors and IntegrateData functions. Dimensionality reduction was performed for visualization; the integrated data were scaled and centered with ScaleData and principal component analysis was performed with RunPCA to reduce the data to 30 principal components (PCs). RunUMAP was then run on the PCs.

Unsupervised clustering and annotation: The FindClusters algorithm was run on the PCs with a resolution of 0.45 to identify clusters in the overall cell population. Sub-clustering of epithelial (resolution=0.038) cell populations was analogously performed. The DimPlot function was then used to create UMAPs stratified by treatment group.

Positive conserved cell type markers were identified using the FindAllMarkers function with minimum detection and $\log_2$-fold change (FC) thresholds set to 25% and Bonferroni adjusted $P \leq 0.05$. The markers were used to perform manual annotation and to merge and split clusters when appropriate. The marker genes were sorted by the $\log_2$-FC multiplied by the difference in percent of cells expressed between the cluster and all other cells. The top marker genes were then visualized with Dotplots (ggplot2 package version 3.4.0 (70)), feature plots (FeaturePlot), and heatmaps (ComplexHeatmap package version 2.12.1 (71)).

Gene Ontology enrichment analysis of epithelial cell populations: Epithelial sub-population differentially expressed genes (DEGs) between *Hmox1*$^{fl/fl}$ and *Hmox1*$^{\Delta IEC}$ mice were identified using the FindAllMarkers MAST Hurdle Approach (72) and previously described thresholds. Genes were considered DE if Bonferroni-adjusted significance was less than 0.05. DEGs were then analyzed to determine whether they were enriched relative to all genes in the dataset. Genes were first annotated

to gene ontology (GO) terms with the biomaRt R package (73) and genes without annotations were eliminated.

Statistics. Unless otherwise stated, statistical significance of comparisons was performed using unpaired two-tailed Student's *t* test for two groups or one-way ANOVA for multiple groups followed by Bonferroni or Dunnett's post hoc test using Prism version 9.5 (GraphPad Software). Error bars reflect standard error of the mean unless otherwise stated. Results were considered statistically significant if $P < 0.05$.

Study approval. All animal studies were performed in accordance with protocols approved by the University of Colorado Anschutz Medical Campus and Rocky Mountain Regional VAMC Institutional Animal Care and Use Committees.

Acknowledgments

This work was supported by a U.S. Department of Veterans Affairs BLR&D Service Career Development Award (JCO, BX003865), Univ. of Colorado GI and Liver Innate Immune Program pilot award (JCO), Merit Reviews (SPC, BX002182 and ALT, BX005288) from the U.S. Department of Veterans Affairs BLR&D Service and an R01 (SPC, DK50189) from the National Institutes of Health. There was additional support from a Cancer Center Support Grant (P30CA046934) and the Genomics and Microarray Core Facility at the University of Colorado Comprehensive Cancer Center.

References

1. Olen O, Erichsen R, Sachs MC, Pedersen L, Halfvarson J, Askling J, et al. Colorectal cancer in ulcerative colitis: a Scandinavian population-based cohort study. *Lancet.* 2020;395(10218):123-31.
2. Olen O, Erichsen R, Sachs MC, Pedersen L, Halfvarson J, Askling J, et al. Colorectal cancer in Crohn's disease: a Scandinavian population-based cohort study. *Lancet Gastroenterol Hepatol.* 2020;5(5):475-84.
3. Jess T, Rungoe C, and Peyrin-Biroulet L. Risk of colorectal cancer in patients with ulcerative colitis: a meta-analysis of population-based cohort studies. *Clin Gastroenterol Hepatol.* 2012;10(6):639-45.
4. Aardoom MA, Joosse ME, de Vries ACH, Levine A, and de Ridder L. Malignancy and Mortality in Pediatric-onset Inflammatory Bowel Disease: A Systematic Review. *Inflamm Bowel Dis.* 2018;24(4):732-41.
5. Ekbom A, Helmick C, Zack M, and Adami HO. Ulcerative colitis and colorectal cancer. A population-based study. *N Engl J Med.* 1990;323(18):1228-33.
6. Ekbom A, Helmick C, Zack M, and Adami HO. Increased risk of large-bowel cancer in Crohn's disease with colonic involvement. *Lancet.* 1990;336(8711):357-9.
7. Schroeder KW, Tremaine WJ, and Ilstrup DM. Coated oral 5-aminosalicylic acid therapy for mildly to moderately active ulcerative colitis. A randomized study. *N Engl J Med.* 1987;317(26):1625-9.
8. D'Haens G, Sandborn WJ, Feagan BG, Geboes K, Hanauer SB, Irvine EJ, et al. A review of activity indices and efficacy end points for clinical trials of medical therapy in adults with ulcerative colitis. *Gastroenterology.* 2007;132(2):763-86.
9. Glei M, Klenow S, Sauer J, Wegewitz U, Richter K, and Pool-Zobel BL. Hemoglobin and hemin induce DNA damage in human colon tumor cells HT29 clone 19A and in primary human colonocytes. *Mutat Res.* 2006;594(1-2):162-71.
10. Seiwert N, Wecklein S, Demuth P, Hasselwander S, Kemper TA, Schwerdtle T, et al. Heme oxygenase 1 protects human colonocytes against ROS formation, oxidative DNA damage and cytotoxicity induced by heme iron, but not inorganic iron. *Cell Death Dis.* 2020;11(9):787.
11. Canesin G, Di Ruscio A, Li M, Ummarino S, Hedblom A, Choudhury R, et al. Scavenging of Labile Heme by Hemopexin Is a Key Checkpoint in Cancer Growth and Metastases. *Cell Rep.* 2020;32(12):108181.
12. Seiwert N, Adam J, Steinberg P, Wirtz S, Schwerdtle T, Adams-Quack P, et al. Chronic intestinal inflammation drives colorectal tumor formation triggered by dietary heme iron in vivo. *Arch Toxicol.* 2021;95(7):2507-22.
13. Knuppel A, Papier K, Fensom GK, Appleby PN, Schmidt JA, Tong TYN, et al. Meat intake and cancer risk: prospective analyses in UK Biobank. *Int J Epidemiol.* 2020;49(5):1540-52.
14. Constante M, Fragoso G, Calve A, Samba-Mondonga M, and Santos MM. Dietary Heme Induces Gut Dysbiosis, Aggravates Colitis, and Potentiates the Development of Adenomas in Mice. *Front Microbiol.* 2017;8:1809.
15. Smith A, and McCulloh RJ. Hemopexin and haptoglobin: allies against heme toxicity from hemoglobin not contenders. *Front Physiol.* 2015;6:187.
16. Ryter SW, Alam J, and Choi AM. Heme oxygenase-1/carbon monoxide: from basic science to therapeutic applications. *Physiol Rev.* 2006;86(2):583-650.
17. Dang D, Meng Z, Zhang C, Li Z, Wei J, and Wu H. Heme induces intestinal epithelial cell ferroptosis via mitochondrial dysfunction in transfusion-associated necrotizing enterocolitis. *FASEB J.* 2022;36(12):e22649.
18. Seiler A, Schneider M, Forster H, Roth S, Wirth EK, Culmsee C, et al. Glutathione peroxidase 4 senses and translates oxidative stress into 12/15-lipoxygenase dependent- and AIF-mediated cell death. *Cell Metab.* 2008;8(3):237-48.

19. Stockwell BR. Ferroptosis turns 10: Emerging mechanisms, physiological functions, and therapeutic applications. *Cell.* 2022;185(14):2401-21.
20. Dixon SJ, Lemberg KM, Lamprecht MR, Skouta R, Zaitsev EM, Gleason CE, et al. Ferroptosis: an iron-dependent form of nonapoptotic cell death. *Cell.* 2012;149(5):1060-72.
21. Dieleman LA, Palmen MJ, Akol H, Bloemena E, Pena AS, Meuwissen SG, and Van Rees EP. Chronic experimental colitis induced by dextran sulphate sodium (DSS) is characterized by Th1 and Th2 cytokines. *Clin Exp Immunol.* 1998;114(3):385-91.
22. Sheikh SZ, Hegazi RA, Kobayashi T, Onyiah JC, Russo SM, Matsuoka K, et al. An anti-inflammatory role for carbon monoxide and heme oxygenase-1 in chronic Th2-mediated murine colitis. *J Immunol.* 2011;186(9):5506-13.
23. Hegazi RA, Rao KN, Mayle A, Sepulveda AR, Otterbein LE, and Plevy SE. Carbon monoxide ameliorates chronic murine colitis through a heme oxygenase 1-dependent pathway. *J Exp Med.* 2005;202(12):1703-13.
24. Onyiah JC, Sheikh SZ, Maharshak N, Steinbach EC, Russo SM, Kobayashi T, et al. Carbon monoxide and heme oxygenase-1 prevent intestinal inflammation in mice by promoting bacterial clearance. *Gastroenterology.* 2013;144(4):789-98.
25. Yang Y, Wang S, Kobayashi K, Hao Y, Kanda H, Kondo T, et al. TRPA1-expressing lamina propria mesenchymal cells regulate colonic motility. *JCI Insight.* 2019;4(9).
26. Zhang X, Li W, Ma Y, Zhao X, He L, Sun P, and Wang H. High-fat diet aggravates colitis-associated carcinogenesis by evading ferroptosis in the ER stress-mediated pathway. *Free Radic Biol Med.* 2021;177:156-66.
27. Planell N, Lozano JJ, Mora-Buch R, Masamunt MC, Jimeno M, Ordas I, et al. Transcriptional analysis of the intestinal mucosa of patients with ulcerative colitis in remission reveals lasting epithelial cell alterations. *Gut.* 2013;62(7):967-76.
28. Barton SG, Rampton DS, Winrow VR, Domizio P, and Feakins RM. Expression of heat shock protein 32 (hemoxygenase-1) in the normal and inflamed human stomach and colon: an immunohistochemical study. *Cell Stress Chaperones.* 2003;8(4):329-34.
29. Paul G, Bataille F, Obermeier F, Bock J, Klebl F, Strauch U, et al. Analysis of intestinal haem-oxygenase-1 (HO-1) in clinical and experimental colitis. *Clin Exp Immunol.* 2005;140(3):547-55.
30. Takagi T, Naito Y, Mizushima K, Nukigi Y, Okada H, Suzuki T, et al. Increased intestinal expression of heme oxygenase-1 and its localization in patients with ulcerative colitis. *J Gastroenterol Hepatol.* 2008;23 Suppl 2:S229-33.
31. Suliman HB, Keenan JE, and Piantadosi CA. Mitochondrial quality-control dysregulation in conditional HO-1(-/-) mice. *JCI Insight.* 2017;2(3):e89676.
32. Madison BB, Dunbar L, Qiao XT, Braunstein K, Braunstein E, and Gumucio DL. Cis elements of the villin gene control expression in restricted domains of the vertical (crypt) and horizontal (duodenum, cecum) axes of the intestine. *J Biol Chem.* 2002;277(36):33275-83.
33. Kanehisa M, and Goto S. KEGG: kyoto encyclopedia of genes and genomes. *Nucleic Acids Res.* 2000;28(1):27-30.
34. Sun Y, Zheng Y, Wang C, and Liu Y. Glutathione depletion induces ferroptosis, autophagy, and premature cell senescence in retinal pigment epithelial cells. *Cell Death Dis.* 2018;9(7):753.
35. Hedblom A, Hejazi SM, Canesin G, Choudhury R, Hanafy KA, Csizmadia E, et al. Heme detoxification by heme oxygenase-1 reinstates proliferative and immune balances upon genotoxic tissue injury. *Cell Death Dis.* 2019;10(2):72.
36. Hayes JD, Dinkova-Kostova AT, and Tew KD. Oxidative Stress in Cancer. *Cancer Cell.* 2020;38(2):167-97.
37. Schwartz AJ, Goyert JW, Solanki S, Kerk SA, Chen B, Castillo C, et al. Hepcidin sequesters iron to sustain nucleotide metabolism and mitochondrial function in colorectal cancer epithelial cells. *Nat Metab.* 2021;3(7):969-82.

38. Singhal R, Mitta SR, Das NK, Kerk SA, Sajjakulnukit P, Solanki S, et al. HIF-2alpha activation potentiates oxidative cell death in colorectal cancers by increasing cellular iron. *J Clin Invest.* 2021;131(12).
39. Tanaka T, Kohno H, Suzuki R, Yamada Y, Sugie S, and Mori H. A novel inflammation-related mouse colon carcinogenesis model induced by azoxymethane and dextran sodium sulfate. *Cancer Sci.* 2003;94(11):965-73.
40. Vega PN, Nilsson A, Kumar MP, Niitsu H, Simmons AJ, Ro J, et al. Cancer-Associated Fibroblasts and Squamous Epithelial Cells Constitute a Unique Microenvironment in a Mouse Model of Inflammation-Induced Colon Cancer. *Front Oncol.* 2022;12:878920.
41. Sirvinskas D, Omrani O, Lu J, Rasa M, Krepelova A, Adam L, et al. Single-cell atlas of the aging mouse colon. *iScience.* 2022;25(5):104202.
42. Haber AL, Biton M, Rogel N, Herbst RH, Shekhar K, Smillie C, et al. A single-cell survey of the small intestinal epithelium. *Nature.* 2017;551(7680):333-9.
43. Gene Ontology C, Aleksander SA, Balhoff J, Carbon S, Cherry JM, Drabkin HJ, et al. The Gene Ontology knowledgebase in 2023. *Genetics.* 2023;224(1).
44. Rodencal J, Kim N, He A, Li VL, Lange M, He J, et al. Sensitization of cancer cells to ferroptosis coincident with cell cycle arrest. *Cell Chem Biol.* 2023.
45. Jardim SR, de Souza LMP, and de Souza HSP. The Rise of Gastrointestinal Cancers as a Global Phenomenon: Unhealthy Behavior or Progress? *Int J Environ Res Public Health.* 2023;20(4).
46. Arnold M, Abnet CC, Neale RE, Vignat J, Giovannucci EL, McGlynn KA, and Bray F. Global Burden of 5 Major Types of Gastrointestinal Cancer. *Gastroenterology.* 2020;159(1):335-49 e15.
47. Zhang R, Kang R, and Tang D. Ferroptosis in gastrointestinal cancer: from mechanisms to implications. *Cancer Lett.* 2023;561:216147.
48. Carlsen CU, Moller JKS, and Skibsted LH. Heme-iron in lipid oxidation. *Coordin Chem Rev.* 2005;249(3-4):485-98.
49. Nam W. High-valent iron(IV)-oxo complexes of heme and non-heme ligands in oxygenation reactions. *Acc Chem Res.* 2007;40(7):522-31.
50. Ijssennagger N, Belzer C, Hooiveld GJ, Dekker J, van Mil SW, Muller M, et al. Gut microbiota facilitates dietary heme-induced epithelial hyperproliferation by opening the mucus barrier in colon. *Proc Natl Acad Sci U S A.* 2015;112(32):10038-43.
51. de Vogel J, van-Eck WB, Sesink AL, Jonker-Termont DS, Kleibeuker J, and van der Meer R. Dietary heme injures surface epithelium resulting in hyperproliferation, inhibition of apoptosis and crypt hyperplasia in rat colon. *Carcinogenesis.* 2008;29(2):398-403.
52. Luu Hoang KN, Anstee JE, and Arnold JN. The Diverse Roles of Heme Oxygenase-1 in Tumor Progression. *Front Immunol.* 2021;12:658315.
53. Adedoyin O, Boddu R, Traylor A, Lever JM, Bolisetty S, George JF, and Agarwal A. Heme oxygenase-1 mitigates ferroptosis in renal proximal tubule cells. *Am J Physiol Renal Physiol.* 2018;314(5):F702-F14.
54. Kwon MY, Park E, Lee SJ, and Chung SW. Heme oxygenase-1 accelerates erastin-induced ferroptotic cell death. *Oncotarget.* 2015;6(27):24393-403.
55. Nishizawa H, Matsumoto M, Shindo T, Saigusa D, Kato H, Suzuki K, et al. Ferroptosis is controlled by the coordinated transcriptional regulation of glutathione and labile iron metabolism by the transcription factor BACH1. *J Biol Chem.* 2020;295(1):69-82.
56. Lv J, Su W, Yu Q, Zhang M, Di C, Lin X, et al. Heme oxygenase-1 protects airway epithelium against apoptosis by targeting the proinflammatory NLRP3-RXR axis in asthma. *J Biol Chem.* 2018;293(48):18454-65.
57. Onyiah JC, Schaefer REM, and Colgan SP. A Central Role for Heme Oxygenase-1 in the Control of Intestinal Epithelial Chemokine Expression. *J Innate Immun.* 2018;10(3):228-38.

58. Wiernicki B, Maschalidi S, Pinney J, Adjemian S, Vanden Berghe T, Ravichandran KS, and Vandenabeele P. Cancer cells dying from ferroptosis impede dendritic cell-mediated anti-tumor immunity. *Nat Commun.* 2022;13(1):3676.
59. Liu J, Zhu S, Zeng L, Li J, Klionsky DJ, Kroemer G, et al. DCN released from ferroptotic cells ignites AGER-dependent immune responses. *Autophagy.* 2022;18(9):2036-49.
60. Angeli JPF, Krysko DV, and Conrad M. Ferroptosis at the crossroads of cancer-acquired drug resistance and immune evasion. *Nat Rev Cancer.* 2019;19(7):405-14.
61. Schneider CA, Rasband WS, and Eliceiri KW. NIH Image to ImageJ: 25 years of image analysis. *Nat Methods.* 2012;9(7):671-5.
62. Schaefer REM, Callahan RC, Atif SM, Orlicky DJ, Cartwright IM, Fontenot AP, et al. Disruption of monocyte-macrophage differentiation and trafficking by a heme analog during active inflammation. *Mucosal Immunol.* 2022;15(2):244-56.
63. Hall CHT, Lee JS, Murphy EM, Gerich ME, Dran R, Glover LE, et al. Creatine Transporter, Reduced in Colon Tissues From Patients With Inflammatory Bowel Diseases, Regulates Energy Balance in Intestinal Epithelial Cells, Epithelial Integrity, and Barrier Function. *Gastroenterology.* 2020;159(3):984-98 e1.
64. van den Berg JW, Koole-Lesuis R, Edixhoven-Bosdijk A, and Brouwers N. Automating the quantification of heme in feces. *Clin Chem.* 1988;34(10):2125-6.
65. Han J, Zhao Q, Basmadjian C, Desaubry L, and Theiss AL. Flavaglines Ameliorate Experimental Colitis and Protect Against Intestinal Epithelial Cell Apoptosis and Mitochondrial Dysfunction. *Inflamm Bowel Dis.* 2016;22(1):55-67.
66. Barrett T, Wilhite SE, Ledoux P, Evangelista C, Kim IF, Tomashevsky M, et al. NCBI GEO: archive for functional genomics data sets--update. *Nucleic Acids Res.* 2013;41(Database issue):D991-5.
67. R Core Team. Vienna, Austria: R Foundation for Statistical Computing; 2022.
68. Hao Y, Hao S, Andersen-Nissen E, Mauck WM, 3rd, Zheng S, Butler A, et al. Integrated analysis of multimodal single-cell data. *Cell.* 2021;184(13):3573-87 e29.
69. McGinnis CS, Murrow LM, and Gartner ZJ. DoubletFinder: Doublet Detection in Single-Cell RNA Sequencing Data Using Artificial Nearest Neighbors. *Cell Syst.* 2019;8(4):329-37 e4.
70. Wickham H. Springer-Verlag New York; 2016.
71. Gu Z, Eils R, and Schlesner M. Complex heatmaps reveal patterns and correlations in multidimensional genomic data. *Bioinformatics.* 2016;32(18):2847-9.
72. Finak G, McDavid A, Yajima M, Deng J, Gersuk V, Shalek AK, et al. MAST: a flexible statistical framework for assessing transcriptional changes and characterizing heterogeneity in single-cell RNA sequencing data. *Genome Biol.* 2015;16:278.
73. Rahnenfuhrer J, and Alexa A. 2022.

Figure Legends

Figure 1. Increased markers of ferroptosis in colitis. WT mice were given DSS 2.5% in their drinking water for 5 days with daily monitoring up to 2 days after DSS was removed (n = 4 per time point). (A) Disease Activity Index (DAI) scoring of mice including weight, bleeding and diarrhea scores. (B) Stool bleeding component of DAI score. (C) Total fecal heme quantification during course of DSS injury. (D-E) Whole colon mRNA expression by RT-qPCR (n = 4-7 mice). (F) Representative photomicrographs of immunohistochemical staining for 4-HNE using paraffin-embedded mouse colon at day 4 of DSS colitis or water only control. (G) Human colonic gene expression values derived from GEO data set GSE38713 microarray data. (H) Human colonic biopsy tissue mRNA expression by RT-qPCR (n = 5 control, 9 UC). *$P < 0.05$, **$P < 0.01$, ***$P < 0.001$, and ****$P < 0.0001$, by unpaired, Student's *t* test or one-way ANOVA for multiple comparisons (compared to day 0 or normal colon).

Figure 2. Colonic epithelial ferroptosis gene response. (A) Photomicrograph of WT C57BL/6 colonoids in Matrigel. (B) Median fluorescence intensity of intact, dissociated colonoid cells stained for 4-HNE, 24h after exposure to hemin (200μM). (C) Colonoid mRNA expression by RT-qPCR after exposure to erastin (20μM) or hemin (100μM) for 24h (n = 4 per group). (D) WT mice were given DSS 2.5% in their drinking water for 5 days with daily monitoring up to 2 days after DSS was removed. HO-1 expression was assessed using intracellular flow cytometry and expressed as a percentage of total IECs (n = 3 per group) with representative gating strategy for IECs, and histogram plots shown. (E) Human colonic biopsy tissue HO-1 assessed by ELISA of tissue homogenates relative to total protein (BCA assay). (F) Representative photomicrograph of non-colitic human-derived colonoids. (G) Colonoid mRNA expression by RT-qPCR after exposure to erastin (20μM) or hemin (100μM). *$P < 0.05$, **$P < 0.01$, ***$P < 0.001$, and ****$P < 0.0001$, by unpaired, Student's *t* test or one-way ANOVA for multiple comparisons (compared to vehicle).

Figure 3. Epithelial *Hmox1* regulates ferroptosis and glutathione metabolism. (A) Representative photomicrograph of colonoids derived from healthy mice. (B) After exposure to hemin (200μM) for 24h,

colonoid cells were dissociated, and flow cytometry was used to measure cell death by uptake of 7-AAD. (C) Principal component analysis 2D plot of colonoid gene expression assessed by RNA sequencing. (D) Venn diagram representation of gene expression patterns in KO and control colonoids. (E) Volcano plot of differentially expressed genes in response to hemin in KO and control colonoids (Up = increased expression in control colonoids). (F) KEGG enrichment analysis of the top 20 most significant gene expression pathways analyzed using hypergeometric test with Benjamini and Hochberg FDR correction. (G) Z-score of gene expression in control and KO colonoids exposed to hemin limited to KEGG glutathione metabolism and ferroptosis pathway genes. ***$P < 0.001$ by one-way ANOVA.

Figure 4. Ferroptosis is induced in murine colonic tumors. (A) Gene expression by RT-qPCR in tumors and adjacent uninvolved colon tissue from AOM-DSS model in WT C57BL/6 mice (n = 5 mice). (B) Representative photomicrograph of immunohistochemical staining for 4-HNE using paraffin-embedded mouse tumor from an AOM-DSS colitis experiment. *$P < 0.05$, **$P < 0.01$, and ***$P < 0.001$, by unpaired, Student's *t* test.

Figure 5. Loss of IEC *Hmox1* decreases intestinal tumorigenesis in AOM-DSS colitis. (A) Scheme of method for azoxymethane-DSS colitis-associated cancer model. (B) Comparison of body weight changes over course of AOM-DSS colitis model in $Hmox1^{fl/fl}$ and $Hmox1^{\Delta IEC}$ mice (n = 8-11 mice per group, pooled from 2 independent experiments). (C) Representative colons with demonstration of tumor formation at day 80 from both mouse strains. (D) – (E) Visible tumor numbers in colon + cecum at day 80 upon gross examination. Combined data from three independent experiments. (F) – (G) Tumor burden and average size as measured by 2-dimensional area of tumor involvement. (H) Number of tumors > 3mm in diameter visualized in colon + cecum at day 80 upon gross examination. (I) Colonic histopathologic injury score at day 80. (J) Representative H&E staining of rectal tumors with adenocarcinoma component. Scale bar is 500 μm for 40x total magnification images and 100 μm for 200x total magnification images. *$p < .05$, **$p < .01$, by unpaired, Student's *t* test.

Figure 6. Increased ferroptosis in tumor epithelial cells from *Hmox1*$^{\Delta IEC}$ tumors. (A) Experimental overview for scRNA-sequencing using tumors from the murine AOM-DSS tumor model. All visible tumors were isolated from individual mice and single cells were enzymatically disassociated followed by sorting of the live population. scRNA-seq was performed using the 10x Genomics platform. (B) UMAP plot of captured cells passing quality control (~24,000) and after unsupervised clustering followed by manual annotation. (C) Dotplot of top-3 marker genes by cluster, ranked according to $\log_2$-FC multiplied by difference in percent expression compared to all other cells. (D) Pie chart reflecting relative fraction of total analyzed cells composed of myeloid, lymphoid and epithelial populations. (E) Proportion of tumor leukocytes relative to total live tumor cells recovered and compared to tumor burden (2nd panel) based on flow cytometry analysis. Results reflect combined data from three independent experiments. (F) List of differentially expressed genes in the tumor epithelial cluster with adjusted $P<0.05$ and $\log_2$FC>0.4 within the *response to oxidative stress* and *glutathione metabolism* GO process group. (G) Tumoroid mRNA expression by RT-qPCR after exposure to hemin (100μM) for 24h (n = 4 per condition). Statistical comparison between *Hmox1*$^{fl/fl}$ and *Hmox1*$^{\Delta IEC}$ per treatment shown. *$P < 0.05$, **$P < 0.01$, ***$P < 0.001$, and ****$P < 0.0001$, by unpaired, Student's *t* test or one-way ANOVA for multiple comparisons.

Figure 1

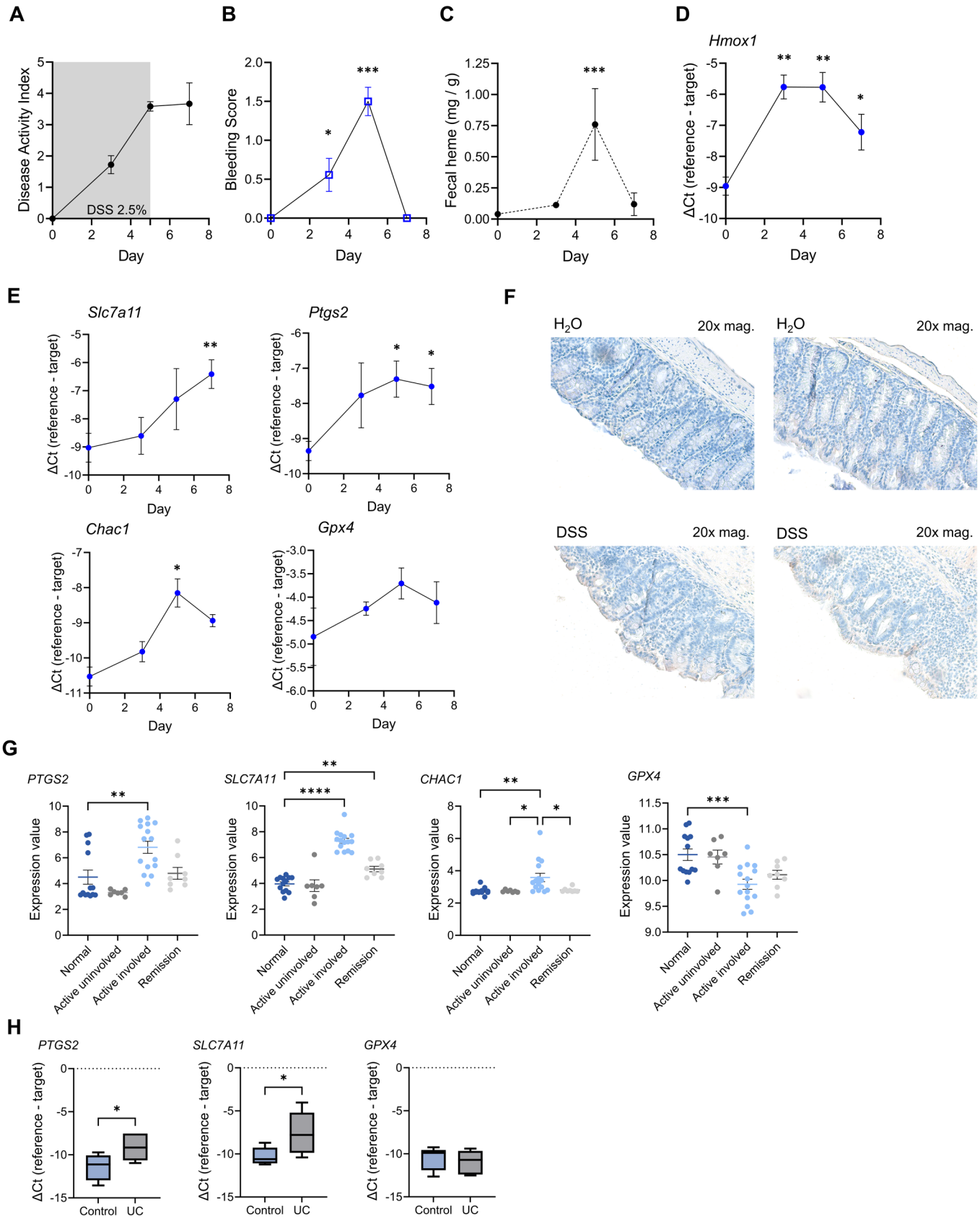
A
Disease Activity Index
DSS 2.5%
Day
B
Bleeding Score
Day
C
Fecal heme (mg / g)
Day
D
Hmox1
ΔCt (reference - target)
Day
E
Slc7a11
Ptgs2
Chac1
Gpx4
ΔCt (reference - target)
Day
F
H2O
20x mag.
DSS
G
PTGS2
SLC7A11
CHAC1
GPX4
Expression value
Normal
Active uninvolved
Active involved
Remission
H
PTGS2
SLC7A11
GPX4
ΔCt (reference - target)
Control
UC

Figure 2

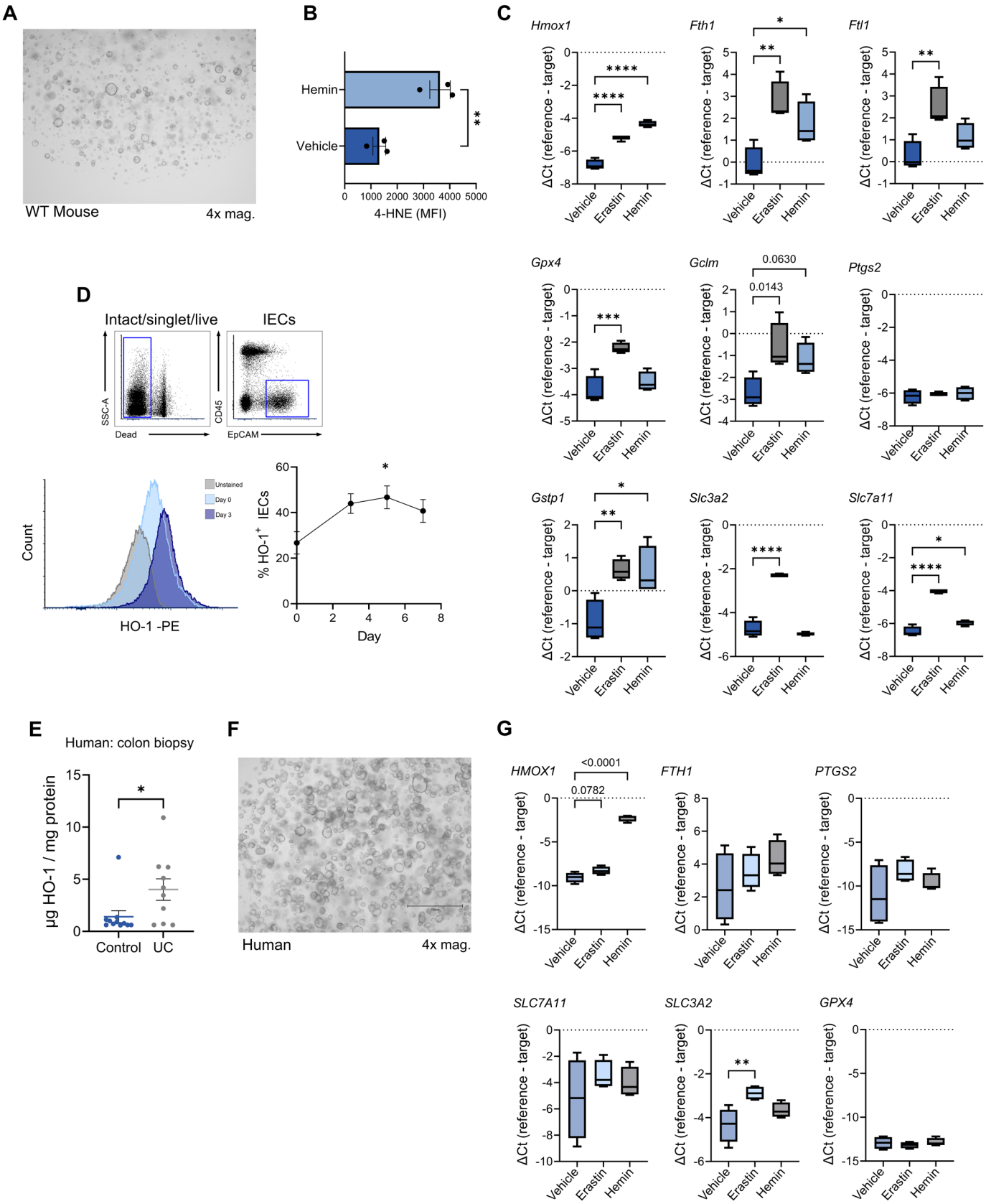
A
WT Mouse
4x mag.
B
Hemin
Vehicle
**
0 1000 2000 3000 4000 5000
4-HNE (MFI)
C
Hmox1
Fth1
Ftl1
Gpx4
Gclm
Ptgs2
Gstp1
Slc3a2
Slc7a11
ΔCt (reference - target)
Vehicle
Erastin
Hemin
0.0630
0.0143
D
Intact/singlet/live
IECs
SSC-A
Dead
CD45
EpCAM
Count
Unstained
Day 0
Day 3
HO-1 -PE
% HO-1+ IECs
Day
E
Human: colon biopsy
µg HO-1 / mg protein
Control
UC
F
Human
4x mag.
G
HMOX1
<0.0001
0.0782
FTH1
PTGS2
SLC7A11
SLC3A2
GPX4

Figure 3

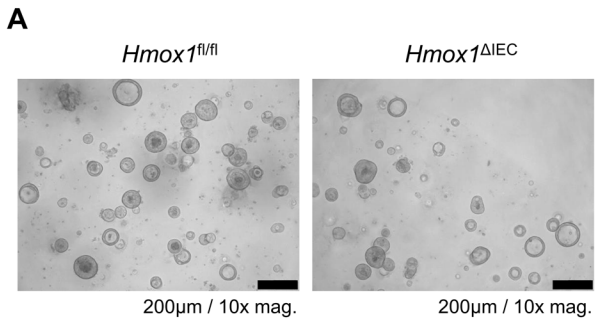
A
Hmox1fl/fl
Hmox1ΔIEC
200µm / 10x mag.
200µm / 10x mag.

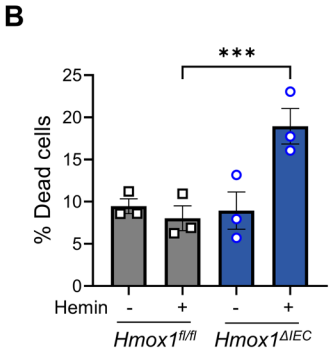
B
***
% Dead cells
25
20
15
10
5
0
Hemin - + - +
Hmox1fl/fl
Hmox1ΔIEC

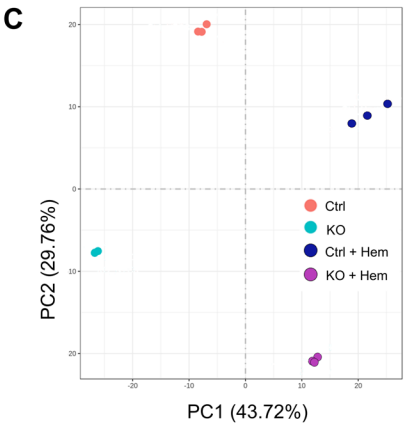
C
Ctrl
KO
Ctrl + Hem
KO + Hem
PC2 (29.76%)
PC1 (43.72%)

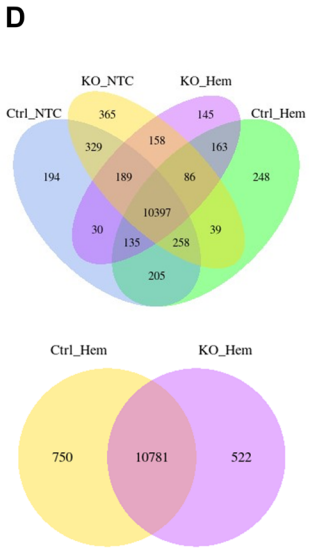
D
KO_NTC
KO_Hem
Ctrl_NTC
Ctrl_Hem
365
145
329
158
163
194
189
86
248
10397
30
39
135
258
205
Ctrl_Hem
KO_Hem
750
10781
522

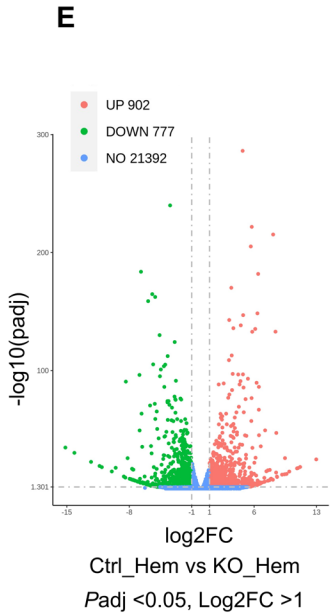
E
UP 902
DOWN 777
NO 21392
-log10(padj)
log2FC
Ctrl_Hem vs KO_Hem
Padj <0.05, Log2FC >1

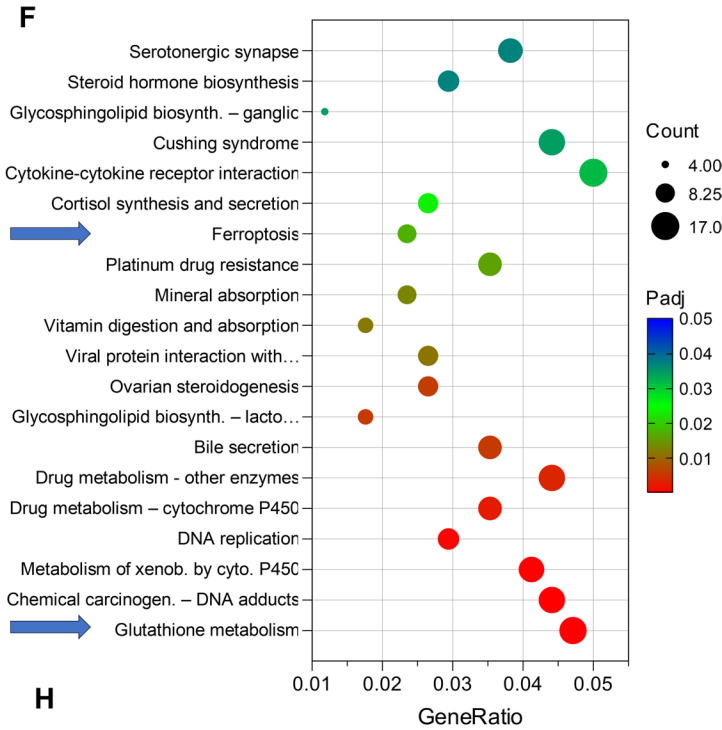
F
Serotonergic synapse
Steroid hormone biosynthesis
Glycosphingolipid biosynth. – ganglic
Cushing syndrome
Cytokine-cytokine receptor interaction
Cortisol synthesis and secretion
Ferroptosis
Platinum drug resistance
Mineral absorption
Vitamin digestion and absorption
Viral protein interaction with…
Ovarian steroidogenesis
Glycosphingolipid biosynth. – lacto…
Bile secretion
Drug metabolism - other enzymes
Drug metabolism – cytochrome P450
DNA replication
Metabolism of xenob. by cyto. P450
Chemical carcinogen. – DNA adducts
Glutathione metabolism
0.01
0.02
0.03
0.04
0.05
GeneRatio
Count
4.00
8.25
17.0
Padj
0.05
0.04
0.03
0.02
0.01

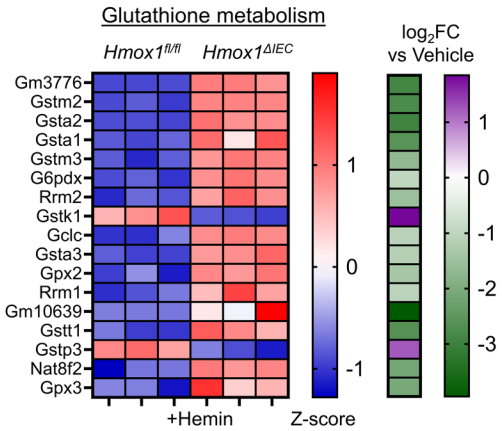
G
Glutathione metabolism
Hmox1fl/fl
Hmox1ΔIEC
Gm3776
Gstm2
Gsta2
Gsta1
Gstm3
G6pdx
Rrm2
Gstk1
Gclc
Gsta3
Gpx2
Rrm1
Gm10639
Gstt1
Gstp3
Nat8f2
Gpx3
+Hemin
Z-score
log2FC
vs Vehicle

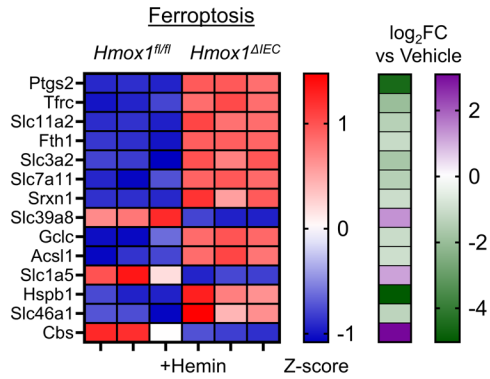
H
Ferroptosis
Hmox1fl/fl
Hmox1ΔIEC
Ptgs2
Tfrc
Slc11a2
Fth1
Slc3a2
Slc7a11
Srxn1
Slc39a8
Gclc
Acsl1
Slc1a5
Hspb1
Slc46a1
Cbs
+Hemin
Z-score
log2FC
vs Vehicle

Figure 4

A

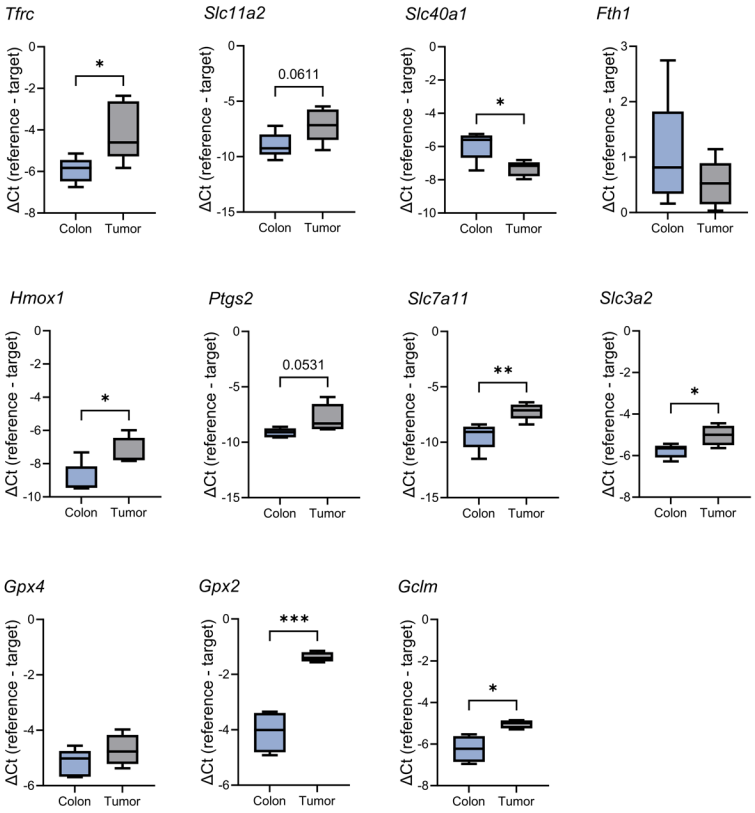
Tfrc
Slc11a2
Slc40a1
Fth1
Hmox1
Ptgs2
Slc7a11
Slc3a2
Gpx4
Gpx2
Gclm
ΔCt (reference - target)
Colon
Tumor
*
0.0611
**
0.0531
***

B

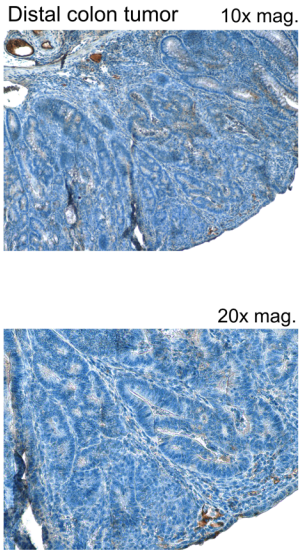
Distal colon tumor
10x mag.
20x mag.

Figure 5

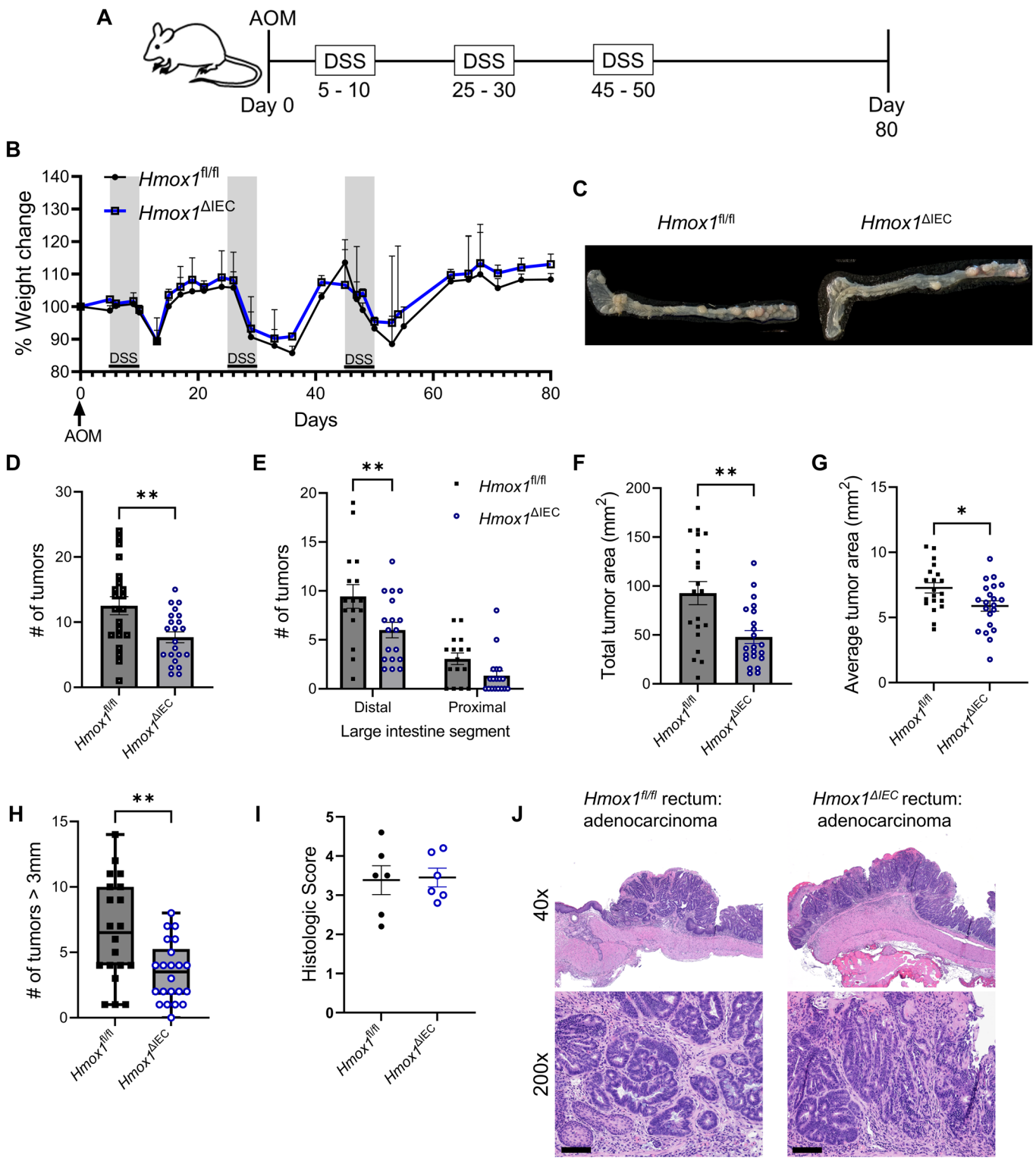
A
AOM
DSS
5 - 10
DSS
25 - 30
DSS
45 - 50
Day 0
Day 80
B
Hmox1fl/fl
Hmox1ΔIEC
% Weight change
DSS
Days
AOM
C
Hmox1fl/fl
Hmox1ΔIEC
D
# of tumors
**
E
# of tumors
Distal
Proximal
Large intestine segment
F
Total tumor area (mm2)
G
Average tumor area (mm2)
H
# of tumors > 3mm
I
Histologic Score
J
Hmox1fl/fl rectum: adenocarcinoma
Hmox1ΔIEC rectum: adenocarcinoma
40x
200x

Figure 6

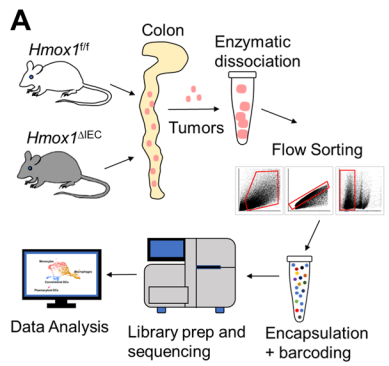
A
Hmox1fl/fl
Hmox1ΔIEC
Colon
Tumors
Enzymatic dissociation
Flow Sorting
Encapsulation + barcoding
Library prep and sequencing
Data Analysis

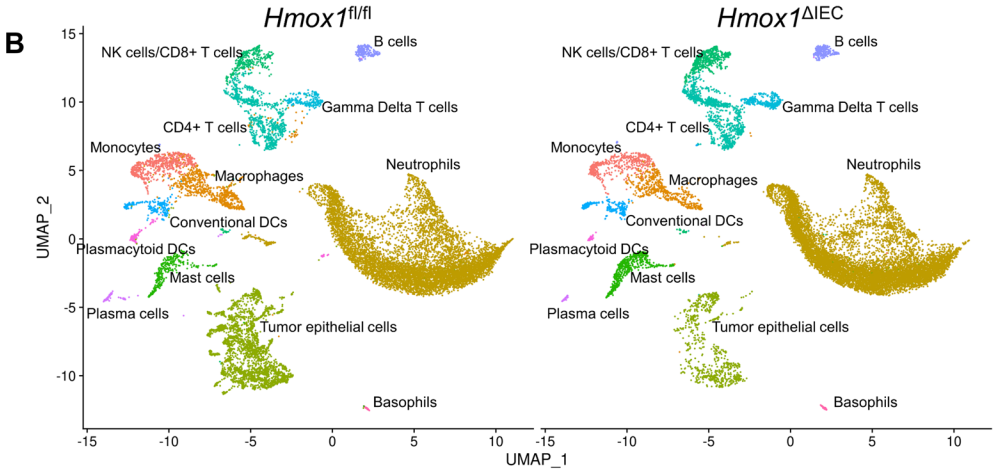
B
Hmox1fl/fl
Hmox1ΔIEC
NK cells/CD8+ T cells
B cells
Gamma Delta T cells
CD4+ T cells
Monocytes
Macrophages
Neutrophils
Conventional DCs
Plasmacytoid DCs
Mast cells
Plasma cells
Tumor epithelial cells
Basophils
UMAP_2
UMAP_1

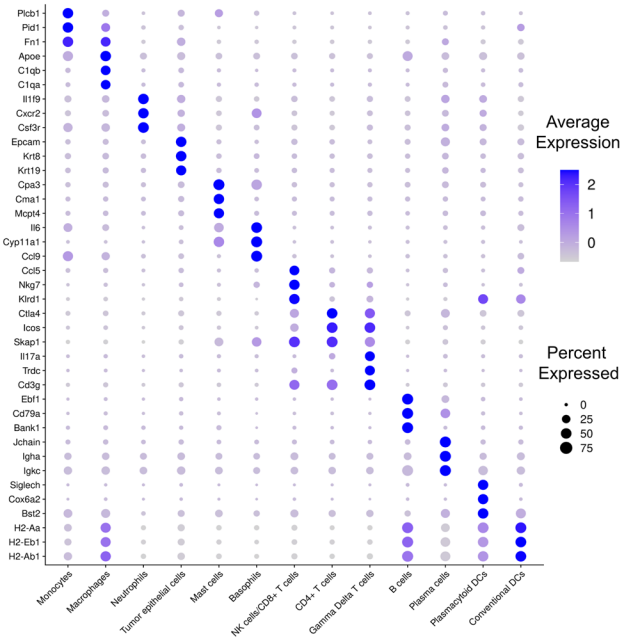
C
Plcb1
Pld1
Fn1
Apoe
C1qb
C1qa
Il1f9
Cxcr2
Csf3r
Epcam
Krt8
Krt19
Cpa3
Cma1
Mcpt4
Il6
Cyp11a1
Ccl9
Ccl5
Nkg7
Klrd1
Ctla4
Icos
Skap1
Il17a
Trdc
Cd3g
Ebf1
Cd79a
Bank1
Jchain
Igha
Igkc
Siglech
Cox6a2
Bst2
H2-Aa
H2-Eb1
H2-Ab1
Monocytes
Macrophages
Neutrophils
Tumor epithelial cells
Mast cells
Basophils
NK cells/CD8+ T cells
CD4+ T cells
Gamma Delta T cells
B cells
Plasma cells
Plasmacytoid DCs
Conventional DCs
Average Expression
Percent Expressed

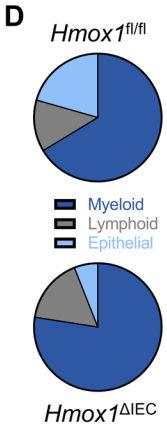
D
Hmox1fl/fl
Hmox1ΔIEC
Myeloid
Lymphoid
Epithelial

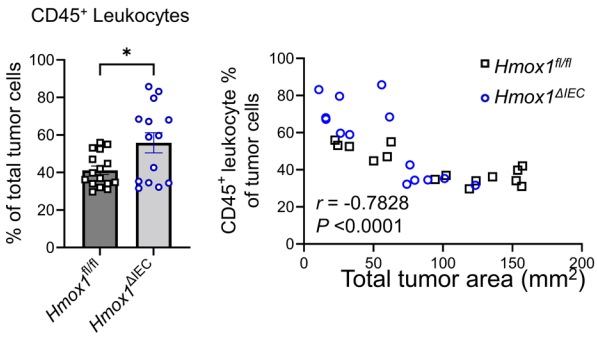
E
CD45+ Leukocytes
% of total tumor cells
Hmox1fl/fl
Hmox1ΔIEC
CD45+ leukocyte % of tumor cells
r = -0.7828
P <0.0001
Total tumor area (mm2)

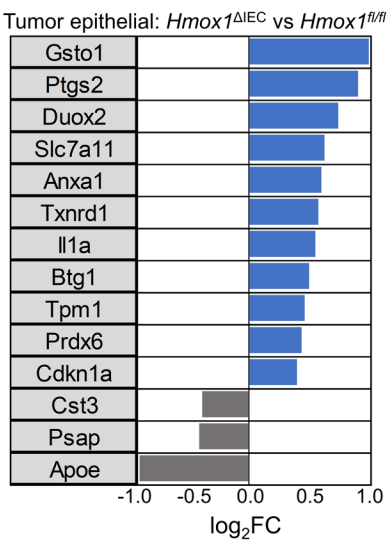
F
Tumor epithelial: Hmox1ΔIEC vs Hmox1fl/fl
Gsto1
Ptgs2
Duox2
Slc7a11
Anxa1
Txnrd1
Il1a
Btg1
Tpm1
Prdx6
Cdkn1a
Cst3
Psap
Apoe
log2FC

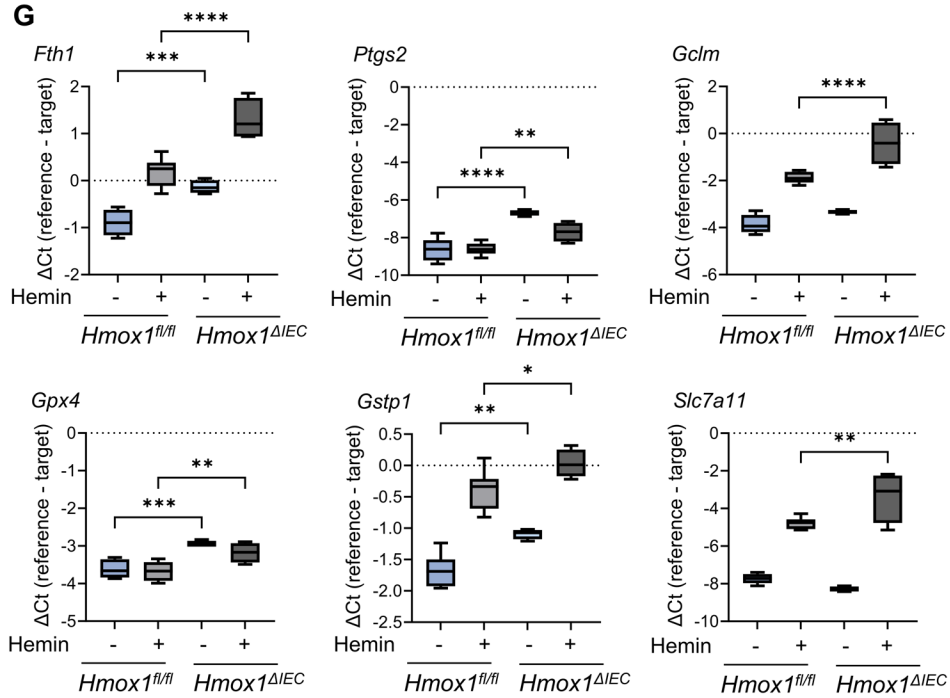
G
Fth1
Ptgs2
Gclm
Gpx4
Gstp1
Slc7a11
ΔCt (reference - target)
Hemin
Hmox1fl/fl
Hmox1ΔIEC